

Multidimensional Probability Density Function Matching for Preprocessing of Multitemporal Remote Sensing Images

Shilpa Inamdar, Francesca Bovolo, *Member, IEEE*, Lorenzo Bruzzone, *Senior Member, IEEE*, and Subhasis Chaudhuri

Abstract—This paper addresses the problem of matching the statistical properties of the distributions of two (or more) multispectral remote sensing images acquired on the same geographical area at different times. An N -D probability density function (pdf) matching technique for the preprocessing of multitemporal images is introduced in the remote sensing domain by defining and analyzing three important application scenarios: 1) supervised classification; 2) partially supervised classification; and 3) change detection. Unlike other methods adopted in remote sensing applications, the procedure considered performs the matching process by properly taking into account the correlation among spectral channels, thus retaining the data correlation structure after the pdf matching. Experimental results obtained on real multitemporal remote sensing data sets confirm the validity of the presented technique in all the considered scenarios.

Index Terms—Change detection, image processing, multidimensional probability density function (pdf) matching, multitemporal images, partially supervised classification, radiometric corrections, remote sensing, supervised classification.

I. INTRODUCTION

THE ANALYSIS of multitemporal images (i.e., images acquired on the same geographical area at different times) is related to some of the most important applications of satellite remote sensing data. On the one hand, supervised or partially supervised classification of temporal series of data is crucial for updating land cover maps of extended geographical areas on a regular basis; on the other hand, supervised or unsupervised change detection in multitemporal images is very important for monitoring of the dynamics of the phenomena that may affect the analyzed area and for risk and damage assessment applications related to natural disasters.

An important observation when dealing with multitemporal images is that they show differences in the statistics that characterize the images acquired at different times. These differences are usually associated with different atmospheric and ground conditions at data acquisition times, as well as instabilities in

sensor calibration. Concerning atmospheric conditions, differences in atmospheric haze, content of water in the atmosphere, etc., may result in significantly different statistics of the images, which affect various spectral channels differently. With regard to the ground conditions, differences in the soil moisture as well as in the phenologic state of the vegetation may significantly affect the radiances measured by multispectral sensors. These critical issues are even more serious if images acquired in different seasons are to be analyzed and compared.

In order to mitigate problems related to the different statistics of the images, three different strategies can be considered [1]: 1) using atmospheric models for defining radiometric corrections techniques that are capable of reducing the undesired effects of the atmosphere; 2) applying calibration techniques based on regression algorithms and ground reference data; and 3) adopting image processing techniques for matching as much as possible the statistical properties of the images in the preprocessing phase. The first two approaches are more appropriate from a theoretical point of view, as they try to derive the spectral reflectance of the land covers by filtering the undesired effects induced from the atmosphere. However, they require additional information for the correction and calibration of the images. In some applications, this information is not available. For these reasons, although preprocessing techniques based on the physics of the atmosphere and/or on ground reference data should be preferred over pure image processing methods (which may affect the radiometry of the scene), in many practical cases, image analysis techniques represent the only reasonable solution to the problem of image corrections. This can be useful both in classification (e.g., for exploiting a classifier trained on an image for classifying another temporal image of the same area) and in change detection (e.g., for reducing false alarms associated with different acquisition conditions of the images).

From an image processing perspective, different approaches can be used to make the statistical properties of pairs of images similar to each other. Among others, we recall the following: 1) linear regression (which is widely used in change detection for predicting the second image starting from the first one and considering the statistical properties of the second image) [2], [3]; 2) nonlinear image normalization (which imposes given values of the mean and of the standard deviation for the corrected image) [4]; and 3) nonlinear histogram shape matching (which performs a matching between the shape of histograms by means of the use of their cumulative histograms).

Manuscript received March 7, 2007; revised August 30, 2007.

S. Inamdar was with the Department of Electrical Engineering, Indian Institute of Technology Bombay, Mumbai 400076, India. She is now with Samsung India Software Operations, Bangalore 560001, India.

F. Bovolo and L. Bruzzone are with the Department of Information and Communication Technologies, University of Trento, 38050 Trento, Italy.

S. Chaudhuri is with the Department of Electrical Engineering, Indian Institute of Technology Bombay, Mumbai 400076, India.

Digital Object Identifier 10.1109/TGRS.2007.912445

This approach is also widely used to solve image mosaicing problems [5]. However, most of these techniques are defined in the context of single-band images and therefore are applied to multispectral images band by band. This represents a critical simplification, as it completely neglects the correlation among bands, which plays an important role in multispectral remote sensing data (images acquired in neighboring portions of the electromagnetic spectrum often have a high correlation that cannot be ignored in the data processing procedures).

To address this problem, in this paper, we introduce, in the remote sensing community, the probability density function (pdf) matching technique proposed in [6] and [7] for multidimensional histogram matching, integrated with the procedure presented in [14] for defining the N -D rotation matrix necessary for matching multidimensional pdf of multispectral images. This method allows one to match the shape of the distributions of two multidimensional images by properly taking into account the correlation among different channels (and, thus, the covariance terms). In particular, we define and analyze three different application scenarios in which the pdf matching procedure can be integrated for generating multispectral images that show statistical distributions as similar as possible to the selected target image. The three scenarios are given as follows: 1) supervised classification of temporal series of images; 2) partially supervised classification of temporal series of images; and 3) unsupervised change detection. All the mentioned scenarios involve the use of algorithms that are associated with the analysis of remote sensing images acquired over the same geographical area at different times. All these algorithms take advantages (in different ways) of the similarity between the statistical properties of the considered multitemporal images.

In the first scenario, the accuracy of a supervised classifier trained on an image and tested on another image (acquired on the same geographical area at a different time) without retraining is analyzed after applying the pdf matching technique. In the second scenario, the pdf matching technique is properly integrated in the partially supervised maximum-likelihood (ML) classifier presented in [8] by modifying the procedure for the initialization of the retraining procedure based on the expectation-maximization (EM) algorithm. In both these scenarios, the rationale of using the probability function transfer technique is related to a typical limitation encountered in the classification of multitemporal images. In particular, since the collection of ground truth is a complex and time-consuming task, often, in the classification of multitemporal images, we have training data for one date but not for the others. In this critical framework, it is important to adopt proper preprocessing algorithms that allow us to transfer the domain knowledge gathered on a particular image (acquired at a given date) to another image (acquired at a different date). Finally, in the third scenario, the effectiveness of the adopted preprocessing technique is analyzed with respect to the solution of an unsupervised change detection problem.

Experimental results obtained on real multitemporal remote sensing images confirm the effectiveness of the considered technique in all the scenarios. In particular, on the selected data set, this technique significantly outperformed the preprocessing capabilities of standard band-by-band histogram shape-matching methods.

This paper is organized into five sections. Section II presents the methodology for the N -D pdf shape matching. Section III describes the data set used in the experiments and the results of the preprocessing phase. Section IV presents the three different analyzed scenarios, i.e., supervised classification, partially supervised classification, and unsupervised change detection, by describing the system setup and experimental results. Finally, Section V draws the conclusions of this paper.

II. N -D PDF MATCHING

A. Problem Formulation and Notation

Let \mathbf{X}_1 and \mathbf{X}_2 be two multispectral images made up of N spectral channels and acquired in the area under analysis at times t_1 and t_2 , respectively. Denote the N -D pdf of the source image \mathbf{X}_1 as $p_1(X)$ and that of the target image \mathbf{X}_2 as $p_2(X)$, where X is an N -D random variable associated with the digital numbers of pixels in a multispectral image. The goal is to find a transfer function that can map function $p_1(X)$ into a new distribution that is as much globally similar as possible to $p_2(X)$. This is achieved without any assumption on the nature of the statistical distributions of the digital numbers in the spectral bands.

For an image with a single spectral band, this problem is much simplified [5], [6] and is known as 1-D transfer (in this paper, we synonymously use the terms 1-D transfer, bandwise pdf matching, and band-by-band pdf matching). The solution is obtained by finding a monotone mapping function $T(X)$ such that

$$T(X) = C_2^{-1} [C_1(X)] \quad (1)$$

where X is, in this particular case, a 1-D random variable, and C_1 and C_2 are the cumulative pdfs of the source and target images, respectively. This problem is solved using discrete lookup tables. For an image with more than one spectral channel, the aforementioned procedure can be independently applied to each band. In this way, it is possible to bring the individual distributions of the bands closer to each other, but the correlations among the spectral bands are neglected. In order to perform a multidimensional pdf transfer, one is required to consider correlations across bands.

The special case of $N = 3$ has received the attention of many researchers in computer graphics. This is widely used when one is required to perform a “touch-up” job on a source image to attain the color shades of a target image. In [9], a technique for matching the means and variances of the target and source images is presented, in which the matching is individually performed on different color channels. Apart from being unable to handle the correlations among various color channels, the method cannot handle any multimodal distribution of the gray levels. Other researchers have proposed improvements to the popular Reinhard algorithm [10]–[12], but they fail to yield a good match of the source and target pdfs in the absence of a proper mechanism to handle correlations among the spectral bands. Recently, Pitié *et al.* have proposed an interesting approach [6], [7] that exploits the properties of the Radon transfer and matches the pdfs of the source and target images by iteratively matching their projections. An extension of the

aforementioned technique to dimensions greater than three is not straightforward, as the Euler-angle-based representation of an N -D rotation matrix adopted in [13] cannot be used. It follows that the generation of an N -D rotation matrix is a nontrivial task [7]. A possible solution would be to randomly draw $N \times N$ matrices and apply *Gram–Schmidt* orthogonalization to generate the desired rotation matrices [7]. However, this procedure does not guarantee the independence between the generated rotations. In Section II-B, we discuss a different but effective way of generating such independent rotation matrices based on the method proposed in [14].

B. N -D PDF Matching Technique

In this section, we briefly recall the N -D pdf matching algorithm procedure presented in [6] and [7] according to the notation introduced in Section II-A.

- 1) Initialize source (\mathbf{X}_1) and target (\mathbf{X}_2) data sets, both with N components corresponding to the N spectral bands.
- 2) Pick a randomly generated $N \times N$ rotation matrix R . (See next section on how this is achieved.)
- 3) At each iteration t , rotate the source image $\mathbf{X}_1(t-1)$ (note that, for $t=1$, the image $\mathbf{X}_1(0)$ corresponds to the original image \mathbf{X}_1) and the target image \mathbf{X}_2 : $\mathbf{X}_1^r(t) \leftarrow R\mathbf{X}_1(t-1)$ and $\mathbf{X}_2^r \leftarrow R\mathbf{X}_2$, where $\mathbf{X}_1^r(t)$ and \mathbf{X}_2^r are the source and target images after rotation in the spectral feature space for the current rotation matrix R , and $\mathbf{X}_1(t-1)$ is the source image after $t-1$ iterations.
- 4) Find the marginal density functions $p_1(X_b^r(t))$ and $p_2(X_b^r)$, $b=1, 2, \dots, N$, by projecting $p_1(X^r(t))$ and $p_2(X^r)$ on each of the N axes in the rotated space.
- 5) For each pair of marginal pdfs, perform 1-D histogram matching on rotated components individually according to (1): $p_1(X_b^r(t))$ to $p_2(X_b^r)$, $b=1, 2, \dots, N$. At the end, the source image is modified, whereas the target one is not.
- 6) Rotate the source image back into the original spectral feature space: $\mathbf{X}_1(t) \leftarrow R^{-1}\mathbf{X}_1^r(t)$.
- 7) Begin the next iteration: $t \leftarrow t+1$, and go to step 2).

The algorithm stops when any further iteration fails to change the pdf of the modified source image in the N -D space. It is possible to prove that the method converges, and at the limit, the pdf of the source image matches that of the target one [6], [7].

C. Generation of the N -D Rotation Matrix

Step 2) in the pdf matching algorithm requires that an N -D rotation matrix R be randomly generated at each iteration. This procedure is very easy for $N=2$, as there is only one independent parameter θ (called the rotation angle, also known as Euler angle). Thus, one is required to randomly generate a value of $\theta(\theta \in [0, 2\pi))$ and to define rotation matrix R as

$$R = \begin{bmatrix} \cos \theta & \sin \theta \\ -\sin \theta & \cos \theta \end{bmatrix}. \quad (2)$$

The same principle is also used for $N=3$, where three Euler angles θ_1 , θ_2 , and θ_3 should be randomly generated.

The corresponding rotation matrix R can be constructed by multiplying three separate rotation matrices as

$$R = R_1 \cdot R_2 \cdot R_3 \quad (3)$$

where

$$R_1 = \begin{bmatrix} \cos \theta_1 & \sin \theta_1 & 0 \\ -\sin \theta_1 & \cos \theta_1 & 0 \\ 0 & 0 & 1 \end{bmatrix}$$

$$R_2 = \begin{bmatrix} 1 & 0 & 0 \\ 0 & \cos \theta_2 & \sin \theta_2 \\ 0 & -\sin \theta_2 & \cos \theta_2 \end{bmatrix}$$

$$R_3 = \begin{bmatrix} \cos \theta_3 & 0 & \sin \theta_3 \\ 0 & 1 & 0 \\ -\sin \theta_3 & 0 & \cos \theta_3 \end{bmatrix}. \quad (4)$$

It is worth noting that, as the matrix multiplication is not commutative, the overall rotation matrix R can be significantly different if the order of multiplications is changed. In either cases of $N=2$ or $N=3$, the rotation matrix is associated with a rotation axis about which a point is rotated by an angle θ . When $N=2$, the rotation axis is always fixed along the direction perpendicular to the plane of rotation. When $N=3$, θ is related to θ_1 , θ_2 , and θ_3 [15]. For $N > 3$, the concept of rotation of an N -D point is difficult to visualize and mathematically formulate, although the interpretation of a unitary matrix in the vector space is quite simple and elegant [14]. The Euler angles in their popular form have no such equivalence in higher dimensions. However, there have been efforts in the area of graphical visualization to use the aforementioned concept of rotation to transform an N -D pattern and then project it into a lower dimensional space for better visualization [10]–[12]. In the following, we describe the method proposed in [14] and adopted in the application scenarios considered in this paper.

An $N \times N$ rotation matrix has degrees of freedom equal to all possible combinations of two that are chosen from a total of N , i.e., ${}^N C_2$. Thus, we need to rotate by ${}^N C_2$ the number of independent angles $(\theta_1, \theta_2, \dots, \theta_{N C_2})$, with each rotation being about an $(N-2)$ -D hyperplane. Since there can be only ${}^N C_2$ linearly independent $(N-2)$ -D hyperplanes, one requires ${}^N C_2$ Euler angles to describe the overall N -D rotation. In the analysis of multispectral remote sensing images, N could be quite large as it represents the number of spectral bands used to acquire the images. For example, $N=6$ for standard Landsat Thematic Mapper (TM) images (neglecting the low-resolution thermal channel); therefore, one requires 15 Euler angles. It is worth noting that this value can become much larger when dealing with hyperspectral images. Once the ${}^N C_2$ independent angular values are defined, the overall rotation matrix R is computed by sequentially multiplying each of the corresponding rotation matrices R_i , $i=1, 2, \dots, {}^N C_2$ [see (5) and (6)]. In order to guarantee that each of these ${}^N C_2$ rotation angles is chosen as independent and uniformly distributed in $[0, 2\pi)$, we adopt the procedure given here for the generation of the random matrix [14].

- 1) Pick ${}^N C_2$ angles $\theta_1, \theta_2, \dots, \theta_{N C_2}$ by random sampling in the uniformly distributed interval of angles $[0, 2\pi)$.

- 2) Generate ${}^N C_2$ matrices $R_1, R_2, \dots, R_{N C_2}$ of size $N \times N$ by considering one angle at a time, each describing a rotation about an $(N - 2)$ -D hyperplane. As an example, for $N = 6$, the matrices will be constructed as follows:

$$R_1 = \begin{bmatrix} \cos \theta_1 & \sin \theta_1 & 0 & 0 & 0 & 0 \\ -\sin \theta_1 & \cos \theta_1 & 0 & 0 & 0 & 0 \\ 0 & 0 & 1 & 0 & 0 & 0 \\ 0 & 0 & 0 & 1 & 0 & 0 \\ 0 & 0 & 0 & 0 & 1 & 0 \\ 0 & 0 & 0 & 0 & 0 & 1 \end{bmatrix},$$

$$R_2 = \begin{bmatrix} 1 & 0 & 0 & 0 & 0 & 0 \\ 0 & \cos \theta_2 & \sin \theta_2 & 0 & 0 & 0 \\ 0 & -\sin \theta_2 & \cos \theta_2 & 0 & 0 & 0 \\ 0 & 0 & 0 & 1 & 0 & 0 \\ 0 & 0 & 0 & 0 & 1 & 0 \\ 0 & 0 & 0 & 0 & 0 & 1 \end{bmatrix},$$

$$R_3 = \begin{bmatrix} 1 & 0 & 0 & 0 & 0 & 0 \\ 0 & 1 & 0 & 0 & 0 & 0 \\ 0 & 0 & \cos \theta_3 & \sin \theta_3 & 0 & 0 \\ 0 & 0 & -\sin \theta_3 & \cos \theta_3 & 0 & 0 \\ 0 & 0 & 0 & 0 & 1 & 0 \\ 0 & 0 & 0 & 0 & 0 & 1 \end{bmatrix}, \dots,$$

$$R_{15} = \begin{bmatrix} \cos \theta_{15} & 0 & 0 & 0 & 0 & \sin \theta_{15} \\ 0 & 1 & 0 & 0 & 0 & 0 \\ 0 & 0 & 1 & 0 & 0 & 0 \\ 0 & 0 & 0 & 1 & 0 & 0 \\ 0 & 0 & 0 & 0 & 1 & 0 \\ -\sin \theta_{15} & 0 & 0 & 0 & 0 & \cos \theta_{15} \end{bmatrix}. \quad (5)$$

- 3) Generate the final rotation matrix R [to be used in step 2) of the pdf matching procedure] of size $N \times N$ as the product of all the preceding ${}^N C_2$ matrices, i.e.,

$$R = R_1 \cdot R_2 \cdot \dots \cdot R_{N C_2}. \quad (6)$$

Remember that, since the matrix multiplications in (6) does not commute, a change in the order of the hyperplanes about which the Euler rotations are carried out will result in a totally different random rotation matrix R . Although this may be important for certain parameter estimation problems, this has no bearing on our application, as we are interested only in generating a set of random rotation matrices.

It is worth noting that, after derotation of the image [step 6)], it is expected that $\mathbf{X}_1(t)$ should lie in the same range as the original image, i.e., 0–255 (or 0–1 in the normalized case). However, during the transformation, a few spurious values may be observed due to numerical inaccuracies. To take care of these results, we applied saturation logic at range boundaries. This may, in principle, introduce slight radiometric distortions for pixels having values at the limit of the dynamic range of the images.

III. DATA SET DESCRIPTION AND PDF TRANSFORMATION RESULTS

Experiments were carried out on a data set made up of two multispectral images acquired by the TM multispectral sensor

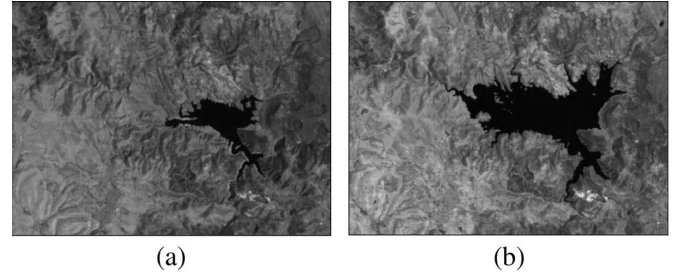


Fig. 1. Bands 5 of the Landsat-5 TM images used for the experiments. (a) Image acquired in September 1995. (b) Image acquired in July 1996.

TABLE I
KL DISTANCE BETWEEN THE DISTRIBUTION ESTIMATED BY DIFFERENT TECHNIQUES AND THE TARGET DISTRIBUTION

Spectral Band	KL distance		
	No pre-processing	Band-by-band pdf transfer	ND pdf transfer
1	0.0858	0.0485	0.03538
2	0.3353	0.0662	0.05479
3	0.4523	0.0419	0.04418
4	0.1517	0.0583	0.04848
5	2.5865	0.0480	0.03848
7	0.0852	0.0741	0.05294

of the Landsat-5 satellite. The selected test site was a section (300×412) of a scene including Mulargia Lake on the Island of Sardinia, Italy. The two images used in the experiments were acquired in September 1995 (t_1) and July 1996 (t_2). The images were coregistered in order to make sure that pixels at the same coordinates in the two images correspond to the same area on ground for validation purposes. The spectral bands 1–5 and 7 were considered in the multispectral images. The thermal channel (i.e., channel 6) is disregarded in these experiments, given its low spatial resolution. As an example, Fig. 1 shows channel 5 of both images. As the images were acquired in different periods of the year, the multidimensional pdf matching problem turned out to be rather complex.

In the experiments, for comparison, both the band-by-band and N -D pdf matching techniques were applied to the aforementioned data set. The new images obtained after band-by-band and N -D pdf transfer are referred to as \mathbf{X}_1^B and \mathbf{X}_1^{N-D} , respectively. In the case of the band-by-band pdf transfer, the pdf of the image \mathbf{X}_1 in each spectral band is matched to that of the respective spectral band of image \mathbf{X}_2 according to (1), without the need for any iteration. For the N -D pdf transfer, 60 iterations of rotations were carried out. The trials were performed using a number of different rotation matrices randomly generated at each run. The reported results are the averages of the statistics computed over ten runs.

We analyzed the pdf transfer results by using the Kullback–Leibler distance (KL distance), which is calculated for the distributions in each spectral band b . The KL distance measure between distribution $p_l(X_b)$ and distribution $p_k(X_b)$ can be computed as follows:

$$D_{lk} = \sum_i p_l(X_b(i)) \log \frac{p_l(X_b(i))}{p_k(X_b(i))} \quad (7)$$

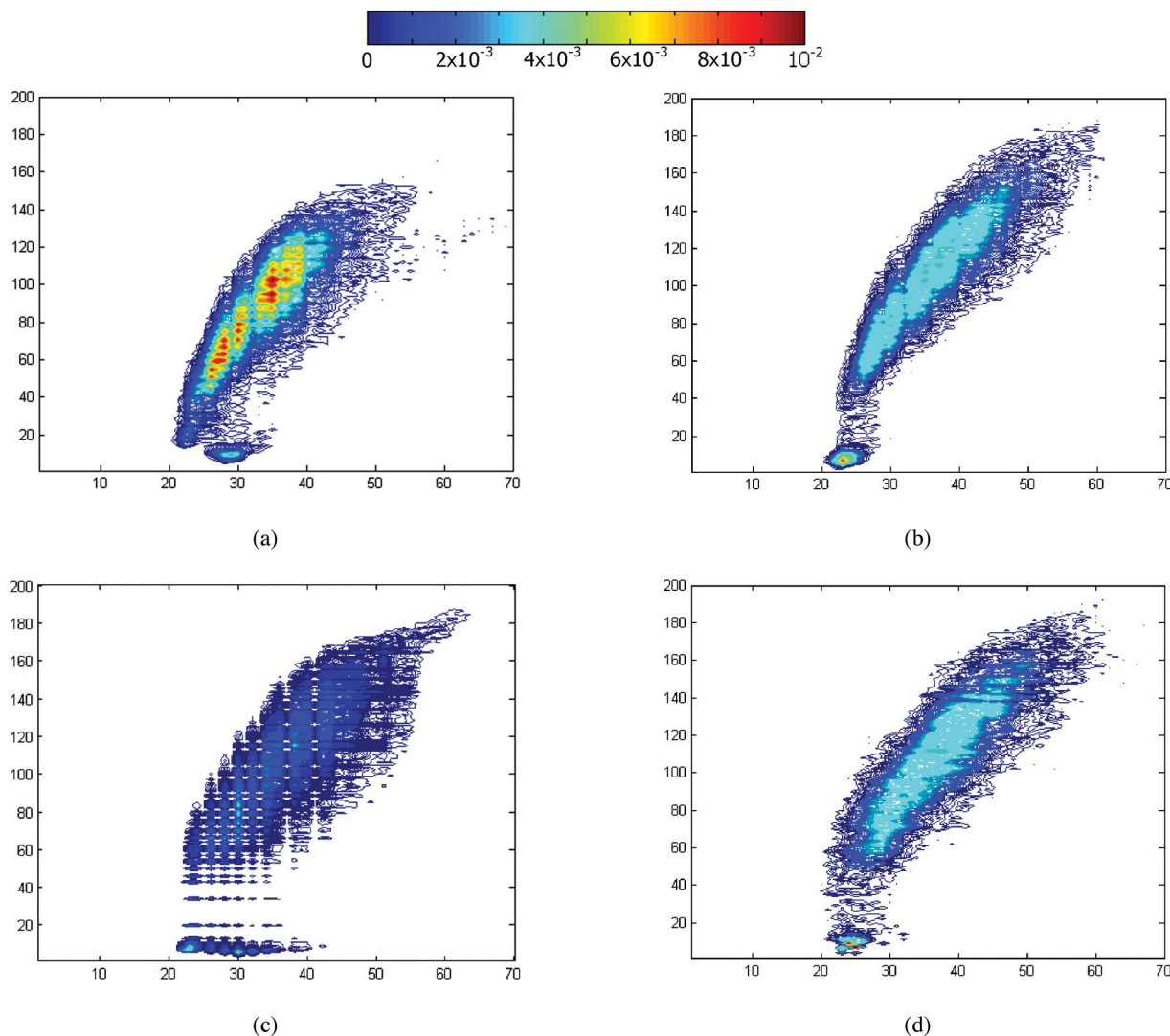


Fig. 2. PDFs in the subspace of spectral bands 3 and 4 of (a) the source image, (b) the target image, (c) the source image after band-by-band histogram matching, and (d) the source image after the presented multidimensional pdf matching.

where i varies in the dynamic range of the considered spectral channel.

The distributions are typically found to be sparse, which results in an unreliable value of the KL distance. This problem of sparseness needs to be handled by smoothing out the distributions. This is achieved by locally interpolating nonzero values over the sparse bins in the histogram. Alternatively, one can use the Epanechnikov kernel, as done in [7]. Since the KL distance is not symmetric, the bidirectional average $D_{avg} = (D_{12} + D_{21})/2$ was considered as the distance between $p_2(X_b)$ and $p_1(X_b)$.

The results obtained after the transformation in terms of KL distance are reported in Table I. From an analysis of the table, one can see that, in general, as expected, the matching process strongly reduces the distances between the histograms of each pair of spectral channels.

In spite of the KL distance being measured bandwise, ignoring the correlation among spectral channels (this implicitly penalizes the evaluation of the effectiveness of the proposed N -D transfer procedure in favor of the bandwise matching procedure), the N -D pdf matching achieves slightly better per-

formances (i.e., a lower distance value) than the 1-D histogram matching.

The qualitative evaluation of the goodness of pdf matching results is performed by visually comparing in the multidimensional domain the shapes of the distributions of the following: 1) the source pdf; 2) the target pdf; 3) the source pdf after band-by-band matching; and 4) the source pdf after the N -D transform. In this paper, for visualization purposes, we present the multidimensional contour plots of two different 2-D subspaces. As representative examples, Figs. 2 and 3 show the projection of the aforementioned multidimensional pdfs on three different subspaces, i.e., bands 3 and 4; and bands 4 and 5, respectively. As expected, in both examples, the source pdf distribution after the N -D transform [Figs. 2(d) and 3(d)] is more similar to the target pdf [Figs. 2(b) and 3(b)] than the ones after band-by-band matching [Figs. 2(c) and 3(c)] or without any preprocessing [Figs. 2(a) and 3(a)]. This confirms that the N -D pdf matching technique is useful in obtaining a transformed image having a multidimensional distribution that is very similar to that of the target one. In addition, it proves that the 1-D transform is unable to properly capture the correlation information associated with

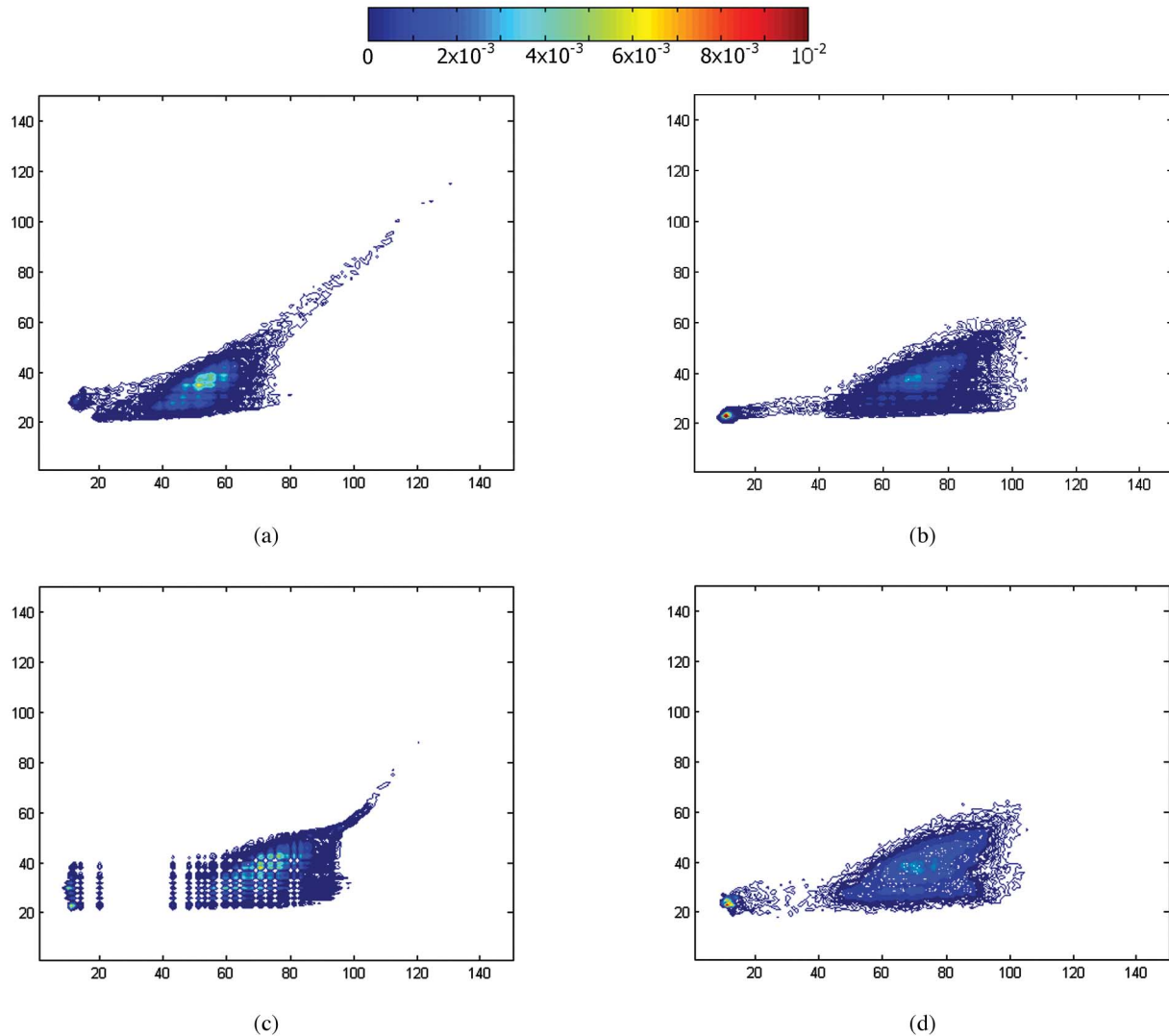


Fig. 3. PDFs in the subspace of spectral bands 4 and 5 of (a) the source image, (b) the target image, (c) the source image after band-by-band histogram matching, and (d) the source image after the presented multidimensional pdf matching.

the multidimensional distributions, leading to poorer matching results. Similar conclusions can be drawn by comparing plots of other subspaces (which are not reported for space constraints).

IV. APPLICATIONS OF THE N -D PDF MATCHING TECHNIQUE

A. Scenario I: Supervised Classification

Supervised classification assumes that training data are available. Although we have a good knowledge of ground truth for both images \mathbf{X}_1 and \mathbf{X}_2 (based on which training and test sets can be derived for both images), in our experiments, we assume that the training data are available only for image \mathbf{X}_1 (i.e., September 1995) and that no training data are available for image \mathbf{X}_2 (i.e., July 1996). The test set at t_2 is considered only for validation purposes. The same set $\Omega = \{\omega_1, \omega_2, \dots, \omega_M\}$ of M land cover classes characterizes the considered geographical area at both t_1 and t_2 . This means that, in our system, only the spatial and spectral distributions of such land cover classes are supposed to vary, and the set of land cover classes

TABLE II
NUMBER OF PATTERNS IN THE TRAINING AND TEST SETS FOR BOTH THE SEPTEMBER 1995 AND JULY 1996 IMAGES

Land-cover class	Number of patterns	
	Training set	Test set
Pasture	554	589
Forest	304	274
Urban area	408	418
Water body	804	551
Vineyard	179	117
Overall	2249	1949

that characterize the considered site is fixed over time. The area is characterized by five land cover classes (i.e., pasture, forest, urban area, water body, and vineyard); hence, $M = 5$ in both images. A detailed description of the training and test set composition is given in Table II. In the experiments reported in this section, it is assumed that the classes have a Gaussian distribution. Thus, each class can be uniquely described by mean vector μ_j and covariance matrix Σ_j of the considered class ω_j . Supervised classification is carried out according to the standard ML technique.

The classifier for the September 1995 image is developed in a supervised way using the available training set. As expected, it gives a high accuracy (90.97%) when applied to the September 1995 test set. We used this supervised classifier trained for the image at t_1 for classifying the image at time t_2 without any additional training (ignoring the availability of the training set at t_2). In greater detail, we carried out three experiments. In the first experiment, the classifier for image \mathbf{X}_1 was directly applied to the classification of image \mathbf{X}_2 . In the second experiment, image \mathbf{X}_1^B (obtained after band-by-band pdf matching) was used for training the classifier with the t_1 training set, thus obtaining a classifier matched to the properties of the t_2 image. In the third experiment, image \mathbf{X}_1^{N-D} (obtained after N -D ($N = 6$) pdf matching) was used, instead of image \mathbf{X}_1^B , for training the classifier and then applied to image \mathbf{X}_2 .

In order to have a classifier that shows a high classification accuracy for two images acquired on the same area at different times, we need to make sure that land cover classes at the two acquisition dates have as similar as possible distributions. We evaluated the similarity between the distributions of classes (before and after the band-by-band and N -D pdf matching) by computing both the Bhattacharya distance between the distributions of each class at the two dates and the average Bhattacharya distance among all the classes. This procedure allows proper consideration of the correlation information and results in a further tool for better assess of the effectiveness of the probability function transfer technique in matching the distributions of classes. The Bhattacharya distance between the distributions of class ω_j at the two acquisition dates t_1 and t_2 (i.e., $p_1(X|\omega_j)$ and $p_2(X|\omega_j)$) is given by

$$B_j = -\ln \left\{ \int_X \sqrt{p_1(X|\omega_j)p_2(X|\omega_j)} dX \right\}. \quad (8)$$

Under the assumption that the classes have a Gaussian distribution, this distance can be calculated as

$$B_j = \frac{1}{8}(\mu_{j,1} - \mu_{j,2})^t \left(\frac{\Sigma_{j,1} + \Sigma_{j,2}}{2} \right)^{-1} (\mu_{j,1} - \mu_{j,2}) + \frac{1}{2} \log \left[\frac{\left| \frac{\Sigma_{j,1} + \Sigma_{j,2}}{2} \right|}{\sqrt{\left| \Sigma_{j,1} \right| \left| \Sigma_{j,2} \right|}} \right] \quad (9)$$

where $\mu_{j,1}$, $\mu_{j,2}$, and $\Sigma_{j,1}$, $\Sigma_{j,2}$ are the mean vectors and the covariance matrices for the distributions of ω_j at t_1 and t_2 . From these class-based distances, we can compute the average Bhattacharya distance as follows:

$$B_{\text{avg}} = \sum_{j=1}^M P(\omega_j) B_j \quad (10)$$

where $P(\omega_j)$ is the *a priori* probability of class ω_j , and B_j is the Bhattacharya distance between distributions of class ω_j in \mathbf{X}_1 and \mathbf{X}_2 .

The Bhattacharya distances obtained after applying the different transformation methods are reported in Table III. It can be clearly seen that the average Bhattacharya distance between

TABLE III
CLASS AND AVERAGE BHATTACHARYA DISTANCES BETWEEN THE TARGET DISTRIBUTION AND THE DISTRIBUTION ESTIMATED BY THE CONSIDERED PDF TRANSFORMING STRATEGIES (SCENARIO I—SUPERVISED CLASSIFICATION)

Class	Bhattacharya distances		
	No pre-processing	Band-by-band pdf transfer	Band-by-band pdf transfer
Pasture	3.7951	0.3701	0.3662
Forest	0.5640	0.3500	0.4937
Urban area	1.5690	0.9303	0.6496
Water body	13.8338	15.2475	0.7159
Vineyard	3.4414	0.6912	0.7929
Average distance	6.5151	5.8131	0.5938

TABLE IV
CLASSIFICATION ACCURACIES (IN PERCENT) FOR DIFFERENT PDF TRANSFER STRATEGIES (SCENARIO I—SUPERVISED CLASSIFICATION)

Class	Classification Accuracy (%)		
	No pre-processing	Band-by-band pdf transfer	ND pdf transfer
Pasture	19.52	94.75	91.60
Forest	95.62	87.88	84.69
Urban area	90.43	97.94	97.35
Water body	36.11	2.58	96.81
Vineyard	24.78	17.5	25.77
Overall accuracy	50.43	59.24	88.98

the actual class distributions in the image \mathbf{X}_2 and the class distributions in \mathbf{X}_1^{N-D} is significantly smaller than that associated with the class distributions in \mathbf{X}_1^B . Hence, we can conclude that the N -D pdf transfer significantly outperforms the band-by-band pdf transfer and results into a distribution that is much closer to the target distribution.

Table IV reports the obtained results in terms of classification accuracies. It can be observed that, as expected, after the N -D pdf transfer, the ML classifier trained on \mathbf{X}_1 outperforms the other two classifiers with an overall accuracy of 88.98% against the 50.43% and 59.24% yielded in the first and second experiments, respectively. In greater detail, it is interesting to focus the attention on the results obtained on the most critical class. In the case of the band-by-band pdf transfer, it can be seen that the Bhattacharya distance for class 4 (water body) increases. This is an indication that the estimated distribution for that class is much farther away from the target. This can justify the very poor classification accuracy (2.58%) for water body when applying band-by-band transfer. The cause can be attributed to the fact that the band-by-band matching technique neglects the correlation among the spectral bands. This is confirmed by observing that, after applying the N -D pdf transfer to the images, the accuracy for this class is very high (96.81%) and much higher than the one obtained by the band-by-band transfer. The improvement of the classification results obtained after N -D transfer confirms the effectiveness of the proposed matching technique over standard band-by-band histogram matching.

It is worth noting that, considering that, in real applications, ground truth information is typically available only for one or few acquisition dates (and not for all of them), the use of the N -D transform makes it possible to exploit a classifier trained on an image for which the training and test sets are available for classifying another image (of the same area) for which training and test sets are not available).

B. Scenario II: Partially Supervised Classification

In this section, we address the same classification problem described for the previous scenario according to a more sophisticated approach that is based on the use of a partially supervised classification technique. Partially supervised classification allows the automatic analysis of a remote sensing image for which training data are not available, drawing on the information derived from an image acquired in the same area at a previous time. In greater detail, the classifier parameters obtained by supervised learning on the image with available training data are updated at time t_2 in an unsupervised way on the basis of the statistical distribution of the image to be classified. We expect that the retrained classifier will perform better than the nonretrained one (see scenario I) when applied to the second image. In this scenario, we adopt the partially supervised ML classifier based on the EM algorithm presented in [8] and [17]. This algorithm is very well justified in this framework, as we assume multivariate Gaussian distribution for the land cover classes. We expect that including the N -D pdf matching strategy in the context of the partially supervised ML classifier allows to define better seeds for the EM algorithm and, thus, to obtain both better estimations of the class statistical parameters and higher classification accuracy.

According to [8], the partially supervised ML classifier starts from a supervised ML trained according to the available ground truth at t_1 and applies the EM algorithm to the mean vectors and covariance matrices of the distributions of classes obtained at t_1 . This is done by modeling the distribution of image \mathbf{X}_2 as a mixture composed of as many components as the number of classes. The iterative procedure associated with the EM (which converges when a maximum of the pseudolikelihood of the estimates is reached) is initialized with the parameters estimated at t_1 . However, we expect that the reliability and accuracy of the estimation process of the class distributions at t_2 significantly depend on the accuracy of the initialization values of the statistical parameters. If significant differences between the distributions of classes in \mathbf{X}_1 and \mathbf{X}_2 occur, the process may converge at suboptimal estimates. Taking this observation into account, we carried out two experiments in the partially supervised retraining framework. First, the statistical parameters of classes corresponding to the classifier for image at t_1 are directly used as seeds for retraining the EM and then classifying the image at t_2 (standard initialization proposed in [8]). Second, the N -D pdf matching was applied to image \mathbf{X}_1 with \mathbf{X}_2 as the target, and the parameters were extracted using the training set at t_1 as described in the first scenario. These parameters were used as a new initialization for the EM algorithm. According to the results obtained in scenario I, in this experimental setup, we did not consider the 1-D pdf transfer. In addition, in this case, for both experiments, we analyzed the Bhattacharya distances between the statistical distributions of classes at the two acquisition dates under different preprocessing conditions and the classification accuracies obtained. The results are reported in Tables V and VI.

The Bhattacharya distances between the estimates of the distributions obtained with the standard initialization of the EM and the proposed initialization based on the N -D pdf transfer are comparable. It can be seen that the average Bhattacharya

TABLE V
BHATTACHARYA DISTANCES BETWEEN THE TARGET DISTRIBUTION AND THE DISTRIBUTION ESTIMATED BY THE EM ALGORITHM (PER CLASS AND AVERAGE VALUE) (SCENARIO II—PARTIALLY SUPERVISED CLASSIFICATION)

Class	Bhattacharya distance	
	No pre-processing	N D pdf transfer
Pasture	0.0442	0.0442
Forest	0.0855	0.0799
Urban area	0.0490	0.0268
Water body	0.0361	0.0361
Vineyard	0.3832	0.0651
Average distance	0.07470	0.0446

TABLE VI
CLASSIFICATION ACCURACIES PROVIDED BY THE PARTIALLY SUPERVISED ML CLASSIFIER WITH STANDARD INITIALIZATION OF THE EM ALGORITHM AND INITIALIZATION BASED ON THE PRESENTED N -D PDF TRANSFER (SCENARIO II—PARTIALLY SUPERVISED CLASSIFICATION)

Class	Classification accuracy (%)	
	No pre-processing	N D pdf transfer
Pasture	94.06	97.69
Forest	87.22	86.42
Urban area	93.06	94.88
Water body	100	100
Vineyard	64.10	76.35
Overall accuracy	92.76	94.93
No. of EM iterations	23	17

distance of the classifier with the N -D pdf matching initialization is slightly better than the one obtained at the convergence of the EM algorithm without any pdf transfer. This results in two important observations: 1) The EM algorithm is capable of obtaining good estimates of the class parameters even without any transformation through retraining. 2) The use of the presented N -D pdf transfer decreases the distance between the target and source distributions, reducing the retraining effort. The use of the proposed initialization strategy increased the overall accuracy from 92.76% to 94.93%, with a sharp improvement (from 64.10% to 76.35%) for the vineyard class. Another interesting conclusion concerns the number of iterations required from the EM algorithm for reaching the convergence: the use of a better initialization value decreases by about 20% the number of iterations required to get convergence (17 instead of 23).

These results confirm the effectiveness of the N -D pdf transfer technique and that its use is also significantly advantageous in the partially supervised framework as the classification accuracy notably increases, making the definition of the initial seeds of the EM algorithm more robust and accurate.

C. Scenario III: Unsupervised Change Detection

The third scenario we consider is significantly different from the previous ones. In this case, we focus the attention on the problem of unsupervised change detection. If we analyze the images described in Section III, we can see from Fig. 1 that the extension of the Mulargia Lake between the two considered time instants significantly changed. This gives us the opportunity to study the usefulness of the N -D pdf matching technique as a preprocessing tool to unsupervised change detection. The

TABLE VII

OVERALL ERROR, FALSE ALARMS, AND MISSED ALARMS (IN NUMBER OF PIXELS) RESULTING FROM THE CVA TECHNIQUE APPLIED TO THE ORIGINAL PAIR OF IMAGES, THE PAIR AFTER BAND-BY-BAND TRANSFORMATION, AND PRESENTED N -D TRANSFORMATION (SCENARIO III—UNSUPERVISED CHANGE DETECTION)

Errors	No pre-processing	Band-by-band pdf transfer	N D pdf transfer
False Alarms	1015	1205	604
Missed Alarms	875	504	503
Total errors	1890	1709	1107

goal of the change detection process in this case is to identify the changes occurred in the extension of the lake surface.

In this experimental setup, we considered a technique for change detection based on the change vector analysis procedure [18], [19]. This technique compares pixel by pixel the two multispectral images X_1 and X_2 according to a vector difference operator. Then, the magnitude of the spectral change vectors is computed for deriving the so-called difference image. The thresholding of the difference image results in the change detection map. In our experiments, the decision threshold was derived according to a manual trial-and-error procedure in order to avoid any bias due to the possible errors introduced from automatic thresholding algorithms. In our analysis, to properly test the effectiveness of the presented N -D pdf transform in managing the correlations among spectral channels, we considered all the spectral bands that can be useful in identifying the analyzed kind of change (i.e., bands 1, 2, 4 and 5; band 3 is not considered as it does not contain useful information with respect to the considered kind of change).

Three different experiments were carried out: 1) change detection without any preprocessing; 2) change detection after a band-by-band pdf matching between images X_1 and X_2 ; and 3) change detection after the application of the N -D pdf transform. The results obtained in the three experiments are reported in Table VII in terms of overall error, false alarms, and missed alarms. From an analysis of Table VII, we observe that the matching procedures allow the increase of the accuracy of the change detection process (this confirms what was expected from the theory on the effects of the radiometric corrections on the change detection accuracy obtained by thresholding the magnitude of the spectral change vector [18], [19]). In greater detail, the proposed N -D technique resulted in the lowest overall change detection error, thus confirming its effectiveness also in this change detection scenario.

It is worth noting that, as in all cases in which nonlinear histogram matching is applied to images before direct comparison, possible local distortion introduced by the transformation procedure may result in artifacts in the change detection map. For this reason, the use of the pdf matching before unsupervised change detection should be carefully evaluated on the basis of the considered operative conditions.

V. DISCUSSION AND CONCLUSION

In this paper, an N -D pdf matching technique originally proposed in [6] and [7] (and implemented with the procedure presented in [14] for defining the N -D rotation matrix) has been introduced in the remote sensing domain for the analysis of multitemporal images. This technique (which adapts the

multidimensional histograms of two images by considering correlations among different spectral channels) has been integrated and analyzed in three different scenarios related to the following applications of the analysis of multitemporal images: 1) supervised classification; 2) partially supervised classification; and 3) change detection.

The adopted N -D pdf matching technique exhibits several important properties in relation to multitemporal remote sensing images: 1) It takes into account the correlation among spectral channels in the matching process. 2) It does not assume any parametric model for the multidimensional histograms during the matching process. 3) It is intrinsically suitable for application to any pair of multispectral images, irrespective of the number of spectral channels N . 4) It can also be used for image preprocessing when prior information on atmospheric parameters or ground reference data is not available. The main disadvantages of the method are those common to this kind of procedures: 1) It decreases its effectiveness if the differences in the considered images are not spatially stationary. 2) It cannot address problems related to partial obscurations induced from the presence of clouds.

In all the considered scenarios, the N -D matching technique, due to its capability in properly matching the distributions of the multispectral and multitemporal images, provided very satisfactory results by improving the accuracies of classification and change detection algorithms. From a general viewpoint, we expect that the adopted technique may introduce marginal spectral distortions at range boundaries. Furthermore, it has been demonstrated in [7] that pdf matching may generate unwanted grain noise in transferred images. Both effects may be critical in certain unsupervised change detection problems and classification applications. Thus, the use of the matching procedure as a preprocessing should be carefully evaluated. However, these are drawbacks common to any kind of histogram matching procedure and not peculiar of the specific technique.

ACKNOWLEDGMENT

This work was carried out under the India-Trento Program for Advanced Research (ITPAR) at the University of Trento, Italy, and Indian Institute of Technology, Bombay, India.

REFERENCES

- [1] J. A. Richards and X. Jia, *Remote Sensing Digital Image Analysis: An Introduction*. New York: Springer-Verlag, 1999.
- [2] J. Heo and T. W. Fitzhugh, "A standardized radiometric normalization method for change detection using remotely sensed imagery," *Photogramm. Eng. Remote Sens.*, vol. 66, no. 2, pp. 173–181, Feb. 2000.
- [3] A. Singh, "Digital change detection techniques using remotely-sensed data," *Int. J. Remote Sens.*, vol. 10, no. 6, pp. 989–1003, 1989.
- [4] R. A. Schowengerdt, *Remote Sensing: Models and Methods for Image Processing*, 2nd ed. New York: Academic, 1997.
- [5] R. Gonzalez and R. Woods, *Digital Image Processing*, 2nd ed. Englewood Cliffs, NJ: Prentice-Hall, 2002.
- [6] F. Pitić, A. Kokaram, and R. Dahyot, " N -dimensional probability function transfer and its application to color transfer," in *Proc. IEEE Int. Conf. Comput. Vis.*, Oct. 17–21, 2005, vol. 2, pp. 1434–1439.
- [7] F. Pitić, A. Kokaram, and R. Dahyot, "Automated colour grading using colour distribution transfer," *Comput. Vis. Image Underst.*, vol. 107, no. 1/2, pp. 123–137, Jul./Aug. 2007.
- [8] L. Bruzzone and D. Fernández Prieto, "Unsupervised retraining of a maximum-likelihood classifier for the analysis of multitemporal remote-sensing images," *IEEE Trans. Geosci. Remote Sens.*, vol. 39, no. 2, pp. 456–460, Feb. 2001.

- [9] E. Reinhard, M. Ashikhmin, B. Gooch, and P. Shirley, "Color transfer between images," *IEEE Comput. Graph. Appl.*, vol. 21, no. 5, pp. 34–41, Jul./Aug. 2001.
- [10] M. Grundland and N. A. Dodgson, "Color histogram specification by histogram warping," in *Proc. SPIE—Color Imaging Process., Hardcopy Appl.*, San Jose, CA, Jan. 17–20, 2005, vol. 5667, pp. 610–621.
- [11] S. Xu, Y. Zhang, S. Zhang, and X. Ye, "Uniform color transfer," in *Proc. IEEE ICIP*, Sep. 11–14, 2005, vol. 3, pp. 940–943.
- [12] C. Wang and Y. Huang, "A novel color transfer algorithm for image sequences," *J. Inf. Sci. Eng.*, vol. 20, no. 6, pp. 1039–1056, Nov. 2004.
- [13] B. K. P. Horn, *Robot Vision*. Cambridge, MA: MIT Press, 1986.
- [14] A. Aguilera and R. Perez-Aguila, "General n-dimensional rotations," in *Proc. WSCG SHORT Commun. Papers*, Feb. 2004, pp. 1–8.
- [15] R. Tsai and T. Huang, "Estimating three-dimensional motion parameters of a rigid planar patch," *IEEE Trans. Acoust., Speech, Signal Process.*, vol. ASSP-30, no. 4, pp. 525–534, Aug. 1982.
- [16] G. Strang, *Linear Algebra and Its Applications*, 3rd ed. Fort Worth, TX: Saunders/HBJ, 1988.
- [17] T. K. Moon, "The expectation-maximization algorithm," *IEEE Signal Process. Mag.*, vol. 13, no. 6, pp. 47–60, Nov. 1996.
- [18] F. Bovolo and L. Bruzzone, "A theoretical framework for unsupervised change detection based on change vector analysis in the polar domain," *IEEE Trans. Geosci. Remote Sens.*, vol. 45, no. 1, pp. 218–236, Jan. 2007.
- [19] L. Bruzzone and D. Fernández Prieto, "Automatic analysis of the difference image for unsupervised change detection," *IEEE Trans. Geosci. Remote Sens.*, vol. 38, no. 3, pp. 1170–1182, May 2000.



Shilpa Inamdar received the B.E. degree in electronics and telecommunications from the University of Pune, Maharashtra, India, in 2003 and M.Tech. degree in communication engineering from the Indian Institute of Technology, Bombay, India, in 2007.

From July 2004–June 2007, she was a Research Assistant with the Advanced Techniques for Remote Sensing Image Processing and Recognition Project of the India-Trento Program for Advanced Research. She is currently with Samsung India Software Operations, Bangalore, India, as a software engineer for multimedia applications. Her research interest includes pattern recognition, image and video processing, and multimedia.



Francesca Bovolo (S'05–M'07) received the Laurea (B.S.) and the Laurea Specialistica (M.S.) degrees in telecommunication engineering (*summa cum laude*) and the Ph.D. degree in communication and information technologies from the University of Trento, Trento, Italy, in 2001, 2003, and 2006, respectively.

She is currently with the Pattern Recognition and Remote Sensing Group, Department of Information and Communication Technologies, University of Trento. Her research interests include remote sensing

image processing, particularly change detection in multispectral and SAR images. She conducts research on these topics within the frameworks of several national and international projects. She is a Referee of the *International Journal of Remote Sensing*, the *Photogrammetric Engineering and Remote Sensing* journal, *Remote Sensing of Environment*, and the *Pattern Recognition* journal.

Dr. Bovolo is a Referee for the IEEE TRANSACTIONS ON GEOSCIENCE AND REMOTE SENSING. She has served on the Scientific Committee of the SPIE International Conference on "Signal and Image Processing for Remote Sensing XI" (Stockholm, Sweden, September 2006), and she is a member of the Scientific Committee of the IEEE Fourth International Workshop on the Analysis of Multi-Temporal Remote Sensing Images (MultiTemp 2007; Leuven, Belgium, July 2007) and of the IEEE International Geoscience and Remote Sensing Symposium 2007 (IGARSS'07; Barcelona, Spain, July 2007). She ranked first place in the Student Prize Paper Competition of the 2006 IEEE International Geoscience and Remote Sensing Symposium (Denver, CO, August 2006).



Lorenzo Bruzzone (S'95–M'98–SM'03) received the Laurea (M.S.) degree in electronic engineering (*summa cum laude*) and the Ph.D. degree in telecommunications from the University of Genoa, Genoa, Italy, in 1993 and 1998, respectively.

From 1998 to 2000, he was a Postdoctoral Researcher with the University of Genoa. In 2000, he joined the Department of Information and Communication Technologies, University of Trento, Trento, Italy, where he is currently a Full Professor of telecommunications. He teaches remote sensing, pattern recognition, and electrical communications. He is the Head of the Remote Sensing Laboratory, Department of Information and Communication Technology, University of Trento. He has been an evaluator of project proposals for many different governments (including European Commission) and scientific organizations. He is the author or coauthor of 60 scientific publications in referred international journals, more than 120 papers in conference proceedings, and seven book chapters. He is a Referee for many international journals and has served on the Scientific Committees of several international conferences.

His current research interests include remote sensing image processing and recognition (analysis of multitemporal data, feature selection, classification, regression and estimation, data fusion, and machine learning). He conducts and supervises research on these topics within the frameworks of several national and international projects.

Dr. Bruzzone was a Guest Editor of a special issue of the IEEE TRANSACTIONS ON GEOSCIENCE AND REMOTE SENSING on the subject of the analysis of multitemporal remote sensing images (November 2003). He was the General Chair and Co-Chair of the First and Second IEEE International Workshop on the Analysis of Multi-temporal Remote-Sensing Images (MultiTemp) and is currently a member of the Permanent Steering Committee of this series of workshops. Since 2003, he has been the Chair of the SPIE Conference on Image and Signal Processing for Remote Sensing. From 2004 to 2006, he served as an Associate Editor for the IEEE GEOSCIENCE AND REMOTE SENSING LETTERS. He is currently an Associate Editor for the IEEE TRANSACTIONS ON GEOSCIENCE AND REMOTE SENSING. He is a member of the Scientific Committee of the India-Italy Center for Advanced Research and of the International Association for Pattern Recognition and of the Italian Association for Remote Sensing (AIT). He ranked first place in the Student Prize Paper Competition of the 1998 IEEE International Geoscience and Remote Sensing Symposium (Seattle, July 1998). He was a recipient of Recognition of the IEEE TRANSACTIONS ON GEOSCIENCE AND REMOTE SENSING Best Reviewers in 1999.



Subhasis Chaudhuri was born in Bahutali, India. He received the B.Tech. degree in electronics and electrical communication engineering from the Indian Institute of Technology (IIT), Kharagpur, in 1985, and the M.S. and Ph.D. degrees in electrical engineering from the University of Calgary, Calgary, AB, Canada, and the University of California, San Diego.

In 1990, he joined the IIT, Bombay, India, as an Assistant Professor and is currently a Professor and the Head of the Department of Electrical Engineering. He has also served as a Visiting Professor at the University of Erlangen-Nuremberg, Erlangen, Germany, and the University of Paris XI, Orsay, France. He is the coauthor of the books *Depth From Defocus: A Real Aperture Imaging Approach* (Springer-Verlag, 1999) and *Motion-Free Super-Resolution* (Springer, 2005). He also edited the book *Super-Resolution Imaging* (Kluwer Academic, 2001). His research interests include pattern recognition, image processing, and computer vision.

Prof. Chaudhuri is a Fellow of the Alexander von Humboldt Foundation, Germany; the Indian National Academy of Engineering; and the Indian Academy of Sciences. He was the recipient of the Dr. Vikram Sarabhai Research Award for the year 2001, the Prof. SVC Aiyra Memorial Award and the Swarnajayanti Fellowship both in 2003, and the S.S. Bhatnagar Prize in engineering sciences for the year 2004.